



Surface acoustic wave devices as passive buried sensors

Jean-Michel Friedt, Thibault Retornaz, Sébastien Alzuaga, Thomas Baron,
Gilles Martin, Thierry Laroche, Sylvain Ballandras, Madeleine Griselin,
Jean-Pierre Simonnet

► To cite this version:

Jean-Michel Friedt, Thibault Retornaz, Sébastien Alzuaga, Thomas Baron, Gilles Martin, et al..
Surface acoustic wave devices as passive buried sensors. *Journal of Applied Physics*, 2011, 109 (3),
pp.034905. 10.1063/1.3504650 . hal-00577141

HAL Id: hal-00577141

<https://hal.science/hal-00577141>

Submitted on 20 Feb 2014

HAL is a multi-disciplinary open access archive for the deposit and dissemination of scientific research documents, whether they are published or not. The documents may come from teaching and research institutions in France or abroad, or from public or private research centers.

L'archive ouverte pluridisciplinaire **HAL**, est destinée au dépôt et à la diffusion de documents scientifiques de niveau recherche, publiés ou non, émanant des établissements d'enseignement et de recherche français ou étrangers, des laboratoires publics ou privés.

Surface Acoustic Wave Devices as Passive Buried Sensors

J.-M Friedt* and T. Rétornaz

SENSeOR SAS, Besançon, France

S. Alzuaga, T. Baron, G. Martin, T. Laroche, and S. Ballandras†

FEMTO-ST, UMR 6174 CNRS/UFC/ENSMM/UTBM, Besançon, France

M. Griselin

Laboratoire ThéMA, CNRS, Besançon, France

J.-P. Simonnet

Laboratoire de ChronoEnvironnement,

Université de Franche-Comté, Besançon, France

(Dated: September 28, 2010)

Abstract

Surface Acoustic Wave (SAW) devices are currently used as passive remote-controlled sensors for measuring various physical quantities through a wireless link. Amongst the two main classes of designs – resonator and delay line – the former has the advantage of providing narrow-band spectrum informations and hence appears compatible with an interrogation strategy complying with ISM (Industry-Scientific-Medical) regulations in Radio-Frequency (RF) bands centered around 434, 866 or 915 MHz. Delay-line based sensors require larger bandwidths as they consists of a few interdigitated electrodes excited by short RF pulses with large instantaneous energy and short response delays, but is compatible with existing equipment such as Ground Penetrating RADAR (GPR). We here demonstrate the measurement of temperature using the two configurations, particularly for long-term monitoring using sensors buried in soil. Although we have demonstrated long term stability and robustness of packaged resonators and signal to noise ratio compatible with the expected application, the interrogation range (max 80 cm) is insufficient for most geology or geophysical purposes. We then focus on the use of delay lines, as the corresponding interrogation method is similar to the one used by GPR which allows for RF penetration distances ranging from a few meters to tens of meters and which operates in the lower RF range, depending on soil water content, permittivity and conductivity. Assuming propagation losses in a pure dielectric medium with negligible conductivity (snow or ice), an interrogation distance of about 40 m is predicted, which overcomes the observed limits met when using interrogation methods specifically developed for wireless SAW sensors, and could partly comply with the above-mentioned applications. Although quite optimistic, this estimate is consistent with the signal to noise ratio observed during an experimental demonstration of the interrogation of a delay line buried at a depth of 5 m in snow.

PACS numbers: 07.79-v

Keywords: GPR, SAW, buried sensors, passive wireless device

I. INTRODUCTION

Within the framework of wireless sensors, surface acoustic wave (SAW) piezoelectric devices provide unique performances in terms of robustness and autonomy compared to active devices (better temperature stability compared to Complementary Metal-Oxide-Semiconductor – CMOS – devices, no need for on-board power supply), and larger interrogation distance than Radio-Frequency IDentification – RFID – passive tags. The use of piezoelectric delay lines and resonators for monitoring physical quantities such as temperature, strain, torque and pressure have already been demonstrated^{1–5}. As opposed to CMOS based devices, acoustic sensors relying on a piezoelectric substrate do not exhibit an incoming energy level threshold to work properly.

The operating principle of these devices is based on a first conversion of an incoming electromagnetic wave to an acoustic propagating wave. As the latter is sensitive to its environment (and hence can be optimized to sense a specific physical parameter) its principal characteristics, and mainly the phase velocity, are modulated according to the conditions the sensor is submitted to. Finally, the acoustic energy stored in the sensor is converted back to an electrical signal by direct piezoelectric effect and dissipated as an electromagnetic radiation through the antenna. This signal is captured and analyzed to evaluate the measured physical parameter.

The resulting interrogation range and compliance with existing RADAR systems (Ground Penetrating Radar – GPR⁶) complements the identification capability already familiar to passive IFF (Identify Friend/Foe) systems used since the second world war, with measurement capabilities⁷.

The short interrogation delay (microsecond to millisecond range) of such sensors enables one for fast data refreshing. The SAW device itself is small (typical package size $10\times5\times1\text{ mm}^3$) but the associated radio-frequency (RF) antennas penalize the compactness of the whole sensor, depending on its frequency operation and the nature of its environment. For instance, operation in dense absorbing (organic) media or with metallic surroundings still is a challenge for achieving large interrogation distance.

We have here investigated the use of SAW resonators and delay lines as buried sensors for long term temperature monitoring: while interrogation speed is hardly an issue, the interrogation distance will define the system efficiency and the range of use. For interrogation

distances smaller than 1 meter, applications mainly concern concrete surface properties monitoring⁸, road aging or near surface soil properties monitoring. However, the application range is greatly enhanced if tens-of-meters-range interrogation distances can be reached⁹, since deep soil properties then can be accessed. We report on the long-term monitoring of soil temperature using the two above-mentioned sensor configurations. Although we demonstrate long term stability and robustness of packaged sensors and signal-to-noise ratio compatible with the expected application, the interrogation range (max 80 cm) is insufficient for most geology or geophysics purposes. We then draw our inspiration from the literature concerning Ground Penetrating Radar (GPR)⁶. The latter technique is widely used for monitoring dielectric interfaces in buried structures, with penetration distances depending on the probe electromagnetic pulse duration and dielectric properties of the soil. We focus on providing complementary informations from sensors with interrogation techniques compatible with GPR, following a strategy commonly known as cooperative target¹⁰. We particularly focus on the use of delay lines, as the corresponding interrogation method is similar to the one used by GPR which allows for interrogation distances ranging from a few meters to tens of meters and which operates in the lower RF range, depending on soil water content, permittivity and conductivity. Assuming propagation losses in a pure dielectric medium with negligible conductivity (snow or ice), an interrogation distance of about 40 m is predicted which reveals compliant with geology and geophysics purposes (temperature and stress monitoring for instance). These results were experimentally tested, using a delay line designed to operate around 100 MHz (the actual GPR working frequency) exhibiting a very simple time response (3 bits) as coding was not a purpose of this work. The delay line has been buried in snow and interrogated at various depths up to the maximum experimentally feasible distance of 5 m, which tends to validate the predicted interrogation distance.

II. BURIED RESONATORS AS PASSIVE TEMPERATURE SENSORS

A first set of experiments has been performed using resonator based sensors^{11–13}. Three 434-MHz surface acoustic wave sensors were buried in clay after being connected to dipole antennas. The length of these antennas is adjusted prior to installation in soil assuming a relative permittivity of 10. The purpose of this experiment is to validate the operation of sensors buried in soil and the evolution of the RF link quality over time, as a function of

temperature or climatic conditions (for instance moisture level in soil).

Each sensor is made of two resonators connected in parallel, one reference frequency and one measurement frequency within the 1.7-MHz wide European ISM band, with each resonator designed so that its frequency remains within one half of the allocated frequency band (for temperatures ranging from -20°C to 160°C). Each sensor is packaged and hermetically sealed in 5×5 mm² ceramic packages. The gold-coated contact pads are tin-soldered to the antennas made of 1.6 mm thick FR4 epoxy coated with 30 μm copper. Interrogating these sensors is performed using a custom-designed monostatic pulse mode RADAR system acting as a reflection-mode frequency-sweep network analyzer. The pulse mode operation improves the isolation between the emission and reception steps and hence the interrogation distance, typically a few meters in air¹⁴.

The first observation during installation of the experiment is that an interrogation unit generating 10 dBm, with a detection limit of -70 dBm¹⁴, is unable to detect a usable signal from devices buried only 30 cm deep, consistent with the tabulated electromagnetic propagation losses in clay whose relative permittivity ϵ_r is in the [4..40] range and conductivity σ is in the [2×10^{-3} ..1] S/m range of 1 to 300 dB/m¹⁵, as computed through the exponentially decay loss α of a monochromatic electromagnetic plane wave at pulsation ω propagating in a conducting medium

$$\alpha = \sqrt{\frac{\epsilon_r}{2} \left(\sqrt{1 + \frac{\sigma^2}{\epsilon^2 \omega^2}} - 1 \right)}$$

where $\epsilon = \epsilon_0 \epsilon_r$.

The read out distance is increased by inserting an electromagnetic waveguide (a simple conducting wire) in the hole in the soil near the buried device (Fig. 1). It must be noted that no electrical connection is provided between this metallic wire and the sensor on one side, or the interrogation unit on the other side, meaning that this setup is resistant to soil motion, oxidation or surface disturbances such a lawn mowing (Fig. 1). Another sensor is then buried at a depth of 80 cm and soldered to a RG174 coaxial cable protruding from the hole in the ground as an open feed connexion. All 10 cm diameter holes were refilled with the same clay than the surrounding area and watered to avoid any air gap.

This setup provides *relative temperature* informations (Fig. 2) over time as the sensors had not been calibrated prior to the experiment. Long term drift due to aging of the transducers is reduced through the differential measurement approach: although a single resonator

frequency might drift over time due to surface contamination after packaging^{16,17}, the *differential* approach of measuring a frequency difference between two resonators submitted to the same environment reduces this effect.

The evolution of the temperature provided by the buried sensors is consistent with a sliding average over 9 days of surface temperatures as provided on the web site <http://www.meteociel.fr/> (maximum of the cross-correlation between the experimental data and the averaged values as a function of sliding window length). The result of this experiment running for more than 500 days is exhibited in Fig. 2: the SAW sensors packaged in ceramic housings are resistant to environmental corrosion, and no significant drift or signal loss was observed during the experiment period. The error bars are consistent with a sub-kelvin resolution, typically of the order of ± 0.1 K. The efficiency of the wireless link was validated during night-time measurements (no visual identification of the location of the sensor other than by scanning the interrogation unit antenna over a ~ 1 m² area where the sensor was supposed to be located until a usable RF signal was acquired) or when snow was covering the measurement area.

However, due to the high duty cycle of resonator interrogation (typically 50% emission and 50% reception and signal processing), peak and average RF power are both in the tens to hundreds of milliwatt range, reducing the interrogation range if RF emission regulations are met. On the other hand, ultra-wide band pulse mode RADAR exhibits very low duty cycles, typically 0.1%, associated with high peak powers in the hundreds to thousands of watts. As this interrogation mode is hardly compatible with resonator-based sensor operation, we have considered the possibility of using wide-band SAW devices, *i.e.* delay lines built on lithium niobate, to meet our goal. Hence, we consider in the next section the use of a commercially available GPR unit as interrogation units for buried acoustic delay lines acting as sensors.

III. INTERROGATING DELAY LINES

A. GPR operation

Throughout this presentation, we will focus on the read out of a SAW sensor using a Malå Geoscience (Malå, Sweden) RAMAC GPR equipped in a 100 MHz bistatic configuration.

The simplest implementation of RADAR interrogation units are designed to generate a short – ideally single – pulse including as much energy as possible. This result is achieved in the RF range by slowly loading a capacitor with a high voltage (provided by a switching power supply for embedded designs) and “instantaneously” emptying this energy in an antenna through an avalanche transistor when triggered by a clock pulse. The duration of the energy transfer is defined by the antenna impedance, which is itself influenced by the antenna dimensions and surrounding medium permittivity (Fig. 3). Hence, GPR operation should be considered as fixed wavelength (defined by the antenna dipole dimensions) rather than fixed frequency, since the soil permittivity affects the electromagnetic velocity and hence the pulse central frequency.

In a classical mode of operation, the bistatic GPR unit operates as follows:

1. a radiofrequency pulse is generated by the emitter, for example by triggering the base of an avalanche transistor and letting the current flow from a capacitor loaded with a high voltage (360 V in the case of the RAMAC unit) to the emitting antenna. In this particular case, the peak power in the dipole antenna load ($70\ \Omega$ impedance at resonance) is thus 2 kW.
2. the direct electromagnetic wave propagating on the surface, as well as all the echoes reflected from the dielectric interfaces in the ground, are recorded by the receiving unit at a sampling rate at least 10 times the nominal value of the emitted pulse (in this case a nominal working frequency of 100 MHz), with a sampling triggered by the same signal controlling the base of the avalanche transistor
3. equivalent time sampling reduces the receiving unit cost and bandwidth: the emitted pulse is repeated at a rate slower than the inverse time needed for the pulse to reach the maximum probing depth (10 μ s repetition rate in the case of the RAMAC unit, yielding a maximum probing depth of 850 m considering an electromagnetic velocity in ice of 170 m/ μ s) and the returned signal is recorded after a time interval referenced on the trigger signal and increased by time steps inverse of the wanted sampling frequency. Hence, by delaying the recording time by an additional 250 ps with respect to the trigger signal every new emitted pulse, an equivalent sampling rate of 4 GHz is achieved even with much slower analog to digital converters and low communication bandwidth between the receiving unit and the recording computer.

For a given position of the GPR, a series of time domain return signals is called a GPR trace. Presenting the returned signal power (trace) as a color or grey-scale map is called a scan. Displaying multiple scans side by side for various positions of the GPR unit is called a GPR profile. GPR profile usually maps the evolution over distance of a dielectric interface or obstacle, for example a glacier bedrock (Fig. 3). Our GPR unit performed in agreement with results found in the literature¹⁸, allowing for the identification of an usable signal more than 150 m deep when used on ice to monitor the bedrock interface of a glacier (Fig. 3).

B. GPR for probing acoustic delay lines

Any impedance mismatch between the avalanche transistor output and antenna through a balun will induce ringing and, in classical RADAR applications, unwanted additional oscillations beyond the main pulse. This ringing may be suitable for interrogating delay lines since more than a single pulse is necessary to efficiently load energy into SAW devices, as their pass-band rarely overpasses 10% of their central operating frequency (related to their electro-mechanical coupling). The extreme case is the resonator of quality factor Q which needs Q/π periods (at 434 MHz, $Q \simeq 10000$ which yields about 3500 periods) to be efficiently loaded. The quality factor of the antenna is usually much below this value, of the order of unity, and hence a passive resonator (coaxial line) might be added between the balun and the antenna to store energy and induce enough ringing when interrogating resonators. Furthermore, it is wise to detune the antenna and the resonator to avoid too strong a coupling between these elements¹⁹.

Hence, interrogating delay lines using a RADAR setup includes new challenges. The number of oscillations of the emitted pulse as well as the central frequency are strongly dependent on the permittivity of the surrounding medium. Indeed, the fixed quantity is the emitted signal wavelength which is defined by the size of the dipole antenna of the GPR, while the center frequency is induced by the equivalent permittivity of the air-soil interface. Despite the impact of the environment on the emitted signal, we observe that the emitted signal is so broad in the frequency domain that it will always overlay the relatively narrowband response of the delay line (Fig. 4).

C. Delay line design

The sensor we have designed includes a transducer made of 21 IDT pairs, three mirrors also made of 21 IDT pairs located at distances from the transducer so that the reflected echoes are detected 1.0, 1.3 and 2.8 μs after the excitation pulse. The acoustic wavelength of $\lambda = 40 \mu\text{m}$ yields a central frequency around 100 MHz, matching the pulse length generated by the 100 MHz antenna of the RAMAC GPR unit. The 128-degrees Y-rotated black lithium niobate (pyro-free) substrate was selected for its strong piezoelectric coupling as well as large temperature drift, making it ideal for temperature measurement applications. The free surface acoustic velocity of the Rayleigh wave is 3979 m/s: the delay line aluminum grating parameters correspond to a metallisation ratio $a/p = 0.5$ and a relative height $h/\lambda=2.5\%$ (1 μm thick aluminum layer) (Fig. 4, top-right)²⁰. Although the acoustic sensor itself is less than $1 \times 1 \text{ cm}^2$ in dimensions, the associated 100 MHz antenna is made of a 1 mm-diameter copper-wire dipole of total length 75 cm.

Furthermore, the time stretching strategy used by GPR to achieve such high sampling rates with rather basic electronics is interesting to develop²¹: successive pulses are generated and the response of the environment is monitored after a programmable time delay, which, in the case of a 500 MHz sampling rate, is increased by 2 ns steps at each interrogation iterate. In the case of Malå's RAMAC GPR, the repetition rate is 100 kHz: this time delay of 10 μs between each emitted pulse explains that under favorable conditions, some leftover echo signal from the delay line (up to 10 μs after the excitation pulse has been received by the sensor) is visible *before* the excitation pulse is emitted. This repetition rate also defines the *maximum* time delay of the last echo generated by the delay line sensor. Most interesting to our signal processing strategy, this measurement technique allows for fast sampling at baseband of the received signal as opposed to a demodulated magnitude information which might lack the phase information we will be using for determining accurately the time delay between the emitted excitation pulse and received echoes.

Figs. 5 and 6 show, on the top-left chart, the time evolution of the reflected signal for a sensor located at 50 cm (Fig. 5) and 1 m (Fig. 6) from the receiving antenna: the sensor is located on the surface of a concrete area, away from the emitting antenna. These sensors were heated up from room temperature to 80°C by a 3 Ω power resistor supplied with a 1.5 A current: the temperature T was monitored using a Pt100 temperature probe

glued next to the acoustic delay line. Since the delay lines were patterned on a (YXl)/128° lithium niobate cut with an experimental temperature drift coefficient of -70 ± 2 ppm/K, the echo delay $\Delta\tau$ variation is $\Delta\tau = 70 \times 10^{-6} \tau (T - T_0)$ with T_0 the reference temperature, $\tau = 1.0$ or $1.3 \mu\text{s}$ depending on the reflection delay τ under consideration. This time delay, $\Delta\tau \in [5.5..6.7]$ ns, is observed as a magnitude signal shift of 3 pixels at most when sampled at 500 MHz. However, as shown by Reindl *et al.*²²⁻²⁴, the magnitude information provides a rough estimation of the temperature while the use of the phase in that purpose improves the accuracy, although with a modulo 2π uncertainty. One full phase rotation is easily identified in practical conditions: considering $\tau \leq 2 \mu\text{s}$, a phase rotation of 2π occurs, in our case, when $\Delta\tau=10$ ns, which happens when $\Delta T = 71$ K.

We have thus applied the following algorithm to extract the temperature information from the RADAR recordings:

- roughly identify the echo location using a cross-correlation magnitude maximum between the emitted pulse and the received echoes. The first three maxima are considered since we know our delay line is designed with three reflectors, while four echoes are actually seen in the 0-3.5 μs time interval due to additional reflections on the edges of the chip,
- perform the Fourier transform of the returned echo to identify the frequency range of interest
- the accurate time delay deduced from the position of *the whole echo burst position* is accessible through the phase of the short-term Fourier transform. This value is plotted in the bottom-left graphs of Figs. 5 and 6, and compared to the Pt100 temperature probe recording.

The absolute phase of the Fourier transform, *i.e.* absolute position of the echoes, depends on the distance of the sensor to the receiving antenna, as can be seen at trace 400 of Fig. 6, where the sensor was moved from 1 m from the receiving antenna to 50 cm. Not only does the magnitude of the received signal increase, but more significantly the phase shift of *both* echoes is affected by this signal change. Hence, the phase *difference* between the time delays of the two echoes due to the two mirrors on a same delay line yields a reliable estimate of the temperature variations, and absolute temperature when calibrated. However, since the

noise of the two time delay estimates are uncorrelated, the noise level of the phase difference is equal to the sum of the noises of each phase estimate: while each phase measurement allows to estimate a temperature with sub-kelvin accuracy when the sensor is located at a fixed position, the temperature recorded from a phase *difference* is accurate to a standard deviation of 1.5 K when the sensor is located at a distance of 50 cm from the receiving antenna. This figure degrades when the sensor is moved away from the receiving antenna, to get above 3 K when the sensor is located at 1 m from the receiving antenna (Fig. 6, bottom left, red). This short term noise is strongly reduced by stacking multiple estimates in a sliding average, as can be seen in Fig. 6 where the green line is a sliding average over 10 samples of the red phase-to-temperature conversion from single measurements.

These experiments were performed on concrete, with the distance between the emitting antenna and the receiving antenna equal to 1 m, and the sensor located 50 cm or 1 m from the receiving antenna, *away* from the emitting antenna (which was thus located 1.5 to 2 m from the delay line sensor). Such a configuration is not favorable for efficient coupling since the surface electromagnetic wave is weak with respect to the electromagnetic coupling towards the soil thanks to its strong dielectric permittivity.

Hence, experimenting in a condition favorable to GPR with an environment of low conductivity, provides convenient conditions to assess the practical usage range of these sensors. We buried sensors in 5 m high snowdrifts close to Ny-Alesund (Spitsbergen, Norway) as a representative environment of temperature monitoring of a glacier in a polar environment. The signal to noise ratios up to this depth allows for extracting the echoes returned from the SAW delay line, identifying the relative phase values and hence the temperature (Fig. 7).

D. Range estimate and sensor signal identification

The unusually long delay between the incoming pulse and the echoes returned by the delay line – 1 to 2 microseconds would be associated with reflectors 85 to 170 m deep in ice – allows in most situations for time domain multiplexing, with sensor-associated signals observed in a time window inconsistent with dielectric interfaces. This method for identifying the source of the signal – dielectric interface or acoustic sensor – is reminiscent of Time Division Multiple Access (TDMA) classically user for sharing a single transmission canal amongst multiple

applications.

Considering the usable reflections recorded from ice-rock interfaces more than $d_{interface}=100$ m below the surface (Fig. 3), we wish to estimate the depth²⁵ at which a GPR-like interrogation scheme would be able to detect informations from a buried delay line. Based on the reflection coefficient of the permittivity mismatch at the interface between the two layers and the typical insertion loss of delay lines, we can estimate the range at which a delay line will provide the receiver of the RADAR with enough power for a measurement:

- assuming a plane wave reaching an interface between ice and rock, the Fresnel reflection coefficient R is computed using relative permittivities $\varepsilon_{ice} = 3.1^{26}$ and $\varepsilon_{rock} \simeq 5$ as $R = \left(\frac{\sqrt{\varepsilon_{ice}} - \sqrt{\varepsilon_{rock}}}{\sqrt{\varepsilon_{ice}} + \sqrt{\varepsilon_{rock}}} \right)^2$. We deduce that in this case, the ice-rock interface exhibits an $IL_{interface} = 19$ dB reflection coefficient
- the ice-rock interface hence presents a reflection coefficient much larger than the typical delay line with a S_{11} insertion loss at 35 dB⁵ (Fig. 4), meaning that the delay line must be close to the RADAR to provide a meaningful signal
- the Free Space Propagation Loss (FSPL²⁷) calculation is adapted to the RADAR configuration considering that the SAW target acts as a point like source. Hence, the classical Friis formula stating that the electromagnetic power decays as the distance d squared becomes a fourth power law, while the antenna aperture remains proportional to the electromagnetic wavelength λ : $FSPL_{RADAR}(d) = 10 \times \log_{10} \left(\frac{\lambda^2}{4\pi} \times \frac{1}{(4\pi d^2)^2} \right) = 10 \log_{10} \left(\frac{\lambda^2}{(4\pi)^3 d^4} \right)$.
- in order to assess the range at which the delay line with $IL_{SAW} = 35$ dB insertion loss can be interrogated, we must identify the depth d_{SAW} for which the received power is equal to the one computed previously in the case of the reflection on the bedrock: $FSPL_{RADAR}(d_{interface}) + IL_{interface} = FSPL_{RADAR}(d_{SAW}) + IL_{SAW}$ yielding a computation of d_{SAW} independent on λ and numerical constants:

$$d_{SAW} = d_{interface} \times 10^{(IL_{interface} - IL_{SAW})/40}$$

In our case, since $IL_{SAW} - IL_{interface}=16$ dB, we conclude that the depth at which the acoustic delay line echoes are of the same magnitude than the reflected signal from an ice-rock interface is $d_{SAW} \simeq 40$ m.

The conclusion of this plane wave analysis is that a SAW delay line buried in ice at a depth of 40 m should provide the same signal level than the dielectric interface at 100 m. The delay line signature in an echo *v.s.* antenna position graphics (as shown in Fig. 7 for example) is characterized by multiple hyperbolas translated in time towards greater depths since the acoustic signal is an attenuated replica of the electromagnetic pulse delayed a few microseconds in time. An inter-correlation between the various pulses thus allows an accurate identification of the time delays within the delay line and hence identification of the physical quantity affecting these delays.

Locating the sensor position during a GPR scan is possible through the identification of the hyperbola summit: the reflected signal delay is minimum when the antennas are positioned above the sensor. However, considering a homogeneous medium (in our case ice) with a known electromagnetic velocity c , then the hyperbola equation of the two way time travel $2t$ as a function of antenna position x on the surface is

$$4c^2t^2 - x^2 = d^2$$

for a sensor located at depth d . Hence, beyond the spatial position of the sensor obtained by scanning the GPR instrument, the depth of the point-like sensor is indicated by the hyperbola curvature equal to $\frac{1}{d \times c}$. Furthermore, this curvature provides a unique signature response since the observed delay (including the acoustic delay of several hundreds of nanoseconds, which would account for a depth of several tens of meters if it were due to the electromagnetic propagation speed) is inconsistent with a dielectric reflector located at depth d .

Finally, multiple sensors with different polarizations can be located in common view of the GPR unit¹⁸: we have observed that the strong linear polarization of the pulse emitted by the GPR dipole is able to select the response from a single sensor buried 2 m deep in snow without interference from another similar sensor located about 4 m away and positioned with an orthogonal polarization. This strategy is only possible in the far field range, at a distance of several wavelengths (1.7 m at 100 MHz in ice) from the surface.

IV. CONCLUSION

We have demonstrated that SAW resonators packaged in ceramic packages buried in clay can operate for more than one year with no significant drift or signal quality degradation. Systematic monitoring of these buried devices provides temperature evolutions consistent with surface temperatures. We also have shown that an interrogation unit compliant with the 434 MHz European ISM band allows for interrogating buried sensors at a depth of 80 cm using a coaxial connection, and of 60 cm by promoting the electromagnetic field penetration in soil using a simple conductive wire placed near the sensor and standing out the ground.

We have designed and fabricated a dedicated temperature sensor for use with a 100 MHz ground penetrating RADAR (GPR) unit and demonstrated the ability to record echo signals when the sensor is located at the surface 50 cm and 1 m away from the receiving antenna, as well as buried more than 5 m deep in snow or ice. We have developed the signal processing steps from raw GPR data to extract a temperature informations deduced from the time relative time delay between successive echo pulses.

In order to improve the interrogation depth of sensors, we have analyzed the interrogation strategy of ground penetrating RADARs (GPR), able to detect informations of reflected electromagnetic energy at dielectric interfaces up to 100 m deep at 100 MHz in low loss propagation media such as ice. We extend this result to an estimate of the depth at which a SAW delay line might provide the same amount of reflected energy by compensating the large insertion loss by bringing the sensor closer to the surface: a plane wave calculation of Fresnel reflection coefficient hints a possible depth of 40 m, in agreement with the observed signal to noise ratio achieved when the sensor is located 5 m under the surface.

Acknowledgment

J.-M Friedt would like to thank S. Zhgoon (Moscow Power Engineering Institute, Russia) for fruitful discussions during the 2009 IFCS/EFTF conference. Ground Penetrating Radar measurements on glaciers were performed as part of French National Research Agency (ANR) Hydro-Sensor-FLOWS program under the supervision of D. Laffly, C. Marlin, M.

Griselin and with the help of É. Bernard and A. Saintenoy.

* Electronic address: `jmfriedt@femto-st.fr`

† Electronic address: `ballandr@femto-st.fr`

- ¹ X. Q. Bao, W. B. an V.V. Varadan, and V. Varadan, in *IEEE Ultrasonics Symposium* (1987), pp. 583–585.
- ² L. Reindl, G. Scholl, T. Ostertag, C. Ruppel, W.-E. Bulst, and F. Seifert, in *IEEE Ultrasonics Symposium* (1996), pp. 363–367.
- ³ W. Buff, M. Rusko, M. Goroll, J. Ehrenpfordt, and T. Vandahl, in *IEEE Ultrasonics Symposium* (1997), pp. 359–362.
- ⁴ A. Pohl, R. Steindl, and L. Reindl, *IEEE transactions on instrumentation and measurement* **48**, 1041 (1999).
- ⁵ W. Bulst, G. Fischerauer, and L. Reindl, *IEEE Transactions on Industrial Electronics* **48**, 265 (2001).
- ⁶ D. Daniels, ed., *Ground Penetrating Radar, 2nd Ed.* (The Institution of Electrical Engineers, London, 2004).
- ⁷ M. Rieback, B. Crispo, and A. Tanenbaum, *IEEE Pervasive Computing* **5**, 62 (2006).
- ⁸ G. Clemena, *Handbook on nondestructive testing of concrete, 2nd Ed.* (CRC Press, 2003).
- ⁹ S. Gogineni, D. Tammana, D. Braaten, C. Leuschen, T. Akins, J. Legarsky, P. Kanagaratnam, J. Stiles, C. Allen, , et al., *J. of Geophysical Research* **106**, 3376133772 (2001).
- ¹⁰ C. Allen, K. Shi, and R. Plumb, *IEEE Transactions on Geoscience and Remote Sensing* **36**, 1821 (1998).
- ¹¹ W. Buff, S. Klett, M. Rusko, J. Ehrenpfordt, and M. Goroli, *IEEE transactions on ultrasonics, ferroelectrics, and frequency control* **45**, 1388 (1998).
- ¹² Y. Wen, P. Li, J. Yang, and M. Zheng, *IEEE sensors journal* **4** (2004).
- ¹³ V. Kalinin, in *IEEE Ultrasonics Symposium* (2005), vol. 3, pp. 1452–1455.
- ¹⁴ J.-M. Friedt, C. Droit, G. Martin, and S. Ballandras, *Rev. Sci. Instrum.* **91**, 014701 (2010).
- ¹⁵ J.-L. Davis and A. Annan, *Geophysical Prospecting* **37**, 531 (1989).
- ¹⁶ W. Shreve, in *Ultrasonics Symposium Proceedings* (1977).
- ¹⁷ R. Parker, in *Ultrasonics Symposium Proceedings* (1977).

- ¹⁸ B. Barrett, T. Murray, R. Clark, and K. Matsuoka, J. Geophys. Res. **113**, F04011 (2008).
- ¹⁹ G. Martin, P. Berthelot, J. Masson, W. Daniau, V. Blondeau-Patissier, B. Guichardaz, S. Ballandras, and A. Lambert (2005), pp. 2089–2092.
- ²⁰ S. Ballandras, A. Reinhardt, V. Laude, A. Soufyane, S. Camou, W. Daniau, T. Pastureaud, W. Steichen, R. Lardat, M. Solal, et al., J. Appl. Phys. **96**, 7731 (2004).
- ²¹ S. Kim, A. Haldemann, C. Ulmer, and E. Ng (2006).
- ²² L. Reindl and I. Shrena, IEEE transactions on ultrasonics, ferroelectrics, and frequency control **51** (2004).
- ²³ S. Schuster, S. Scheiblhofer, L. Reindl, and A. Stelzer, IEEE transactions on ultrasonics, ferroelectrics, and frequency control **53** (2006).
- ²⁴ A. Stelzer, S. Schuster, and S. Scheiblhofer, Second International Symposium on Acoustic Wave Devices for Future Mobile Communication Systems (2004).
- ²⁵ G. Leucci, Scholarly research exchange (2008).
- ²⁶ J. Jiang and D. Wu, Atmospheric Science Letters **5**, 146 (2004).
- ²⁷ C. Balanis, *Antenna theory – analysis and design, 2nd Ed.* (John Wiley & Sons, 1997).

Supplementary material

Fig. 8 depicts the experimental setup for measuring the response of SAW delay lines buried 5 m deep in a snowdrift. The sensor and the associated 70 cm long dipole antenna are located in a 3 cm diameter tube filled with snow. The tube is inserted about 1.5 m deep in snow while the GPR scans this area and records both dielectric reflections and echoes from the SAW sensor as a function of antenna position. Although each absolute echo phase with respect to the emitted pulse is dependent on the antenna position, the difference of the phases of the echoes is independent on the antenna position and only depends on the acoustic velocity, or in this case the temperature through the temperature coefficient of frequency of the piezoelectric substrate. The data displayed in Figs. 7 and 8 were processed using the Seismic Unix package (<http://www.cwp.mines.edu/cwpcodes>) with the application of a normalization step and bandpass filtering in the 100 ± 50 MHz band.

Analyzing the signal to noise ratio of the echoes returned – starting $1 \mu\text{s}$ after the emitted pulse and for a duration of $3.3 \mu\text{s}$ – from the sensor buried 5 m deep in snow, one can estimate

the depth at which the minimum signal will be detectable. Considering a signal to noise ratio above 1.7, the maximum readout distance should be 8 times further than the current position (since $1.7^4 \simeq 8$), consistent with the 40 m maximum depth estimated from the classical GPR link budget presented in the main text.

Figures

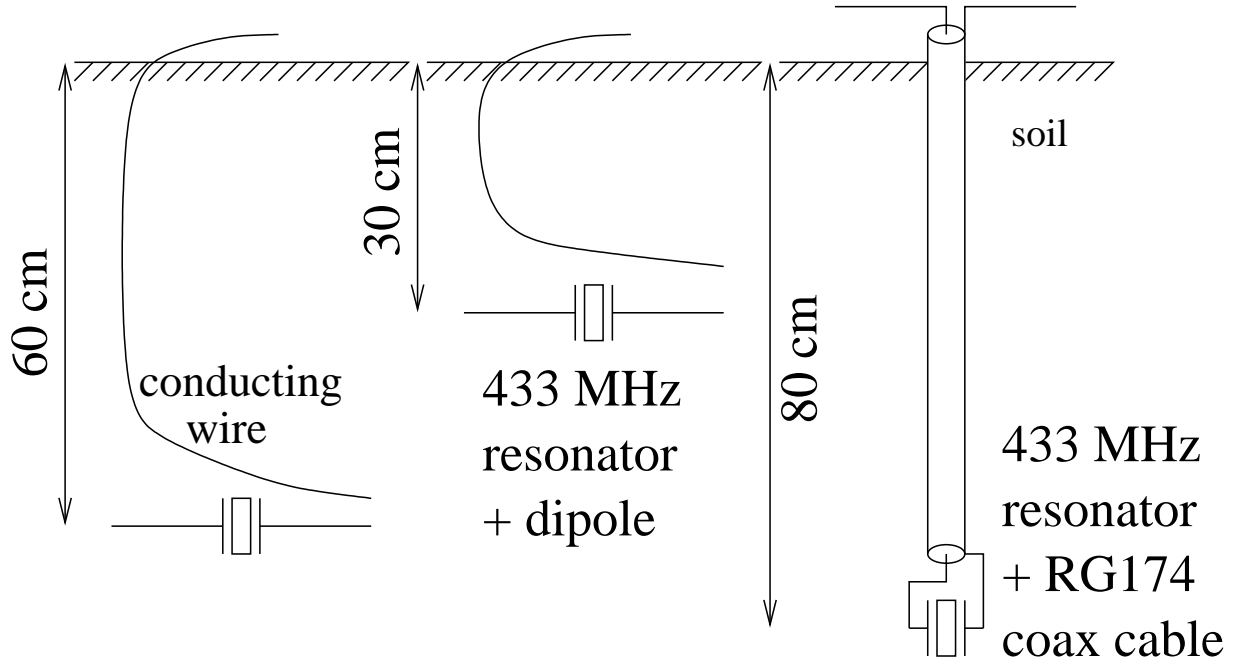


FIG. 1: Experimental configuration: the 30 cm and 60 cm deep devices are SAW resonators soldered to a 2×5 cm long dipole, buried in clay with a conducting wire located in the hole but neither electrically connected to the sensor nor to the interrogation unit. The 80 cm deep resonator was soldered to an RG174 coaxial cable protruding from ground as an open-feed.

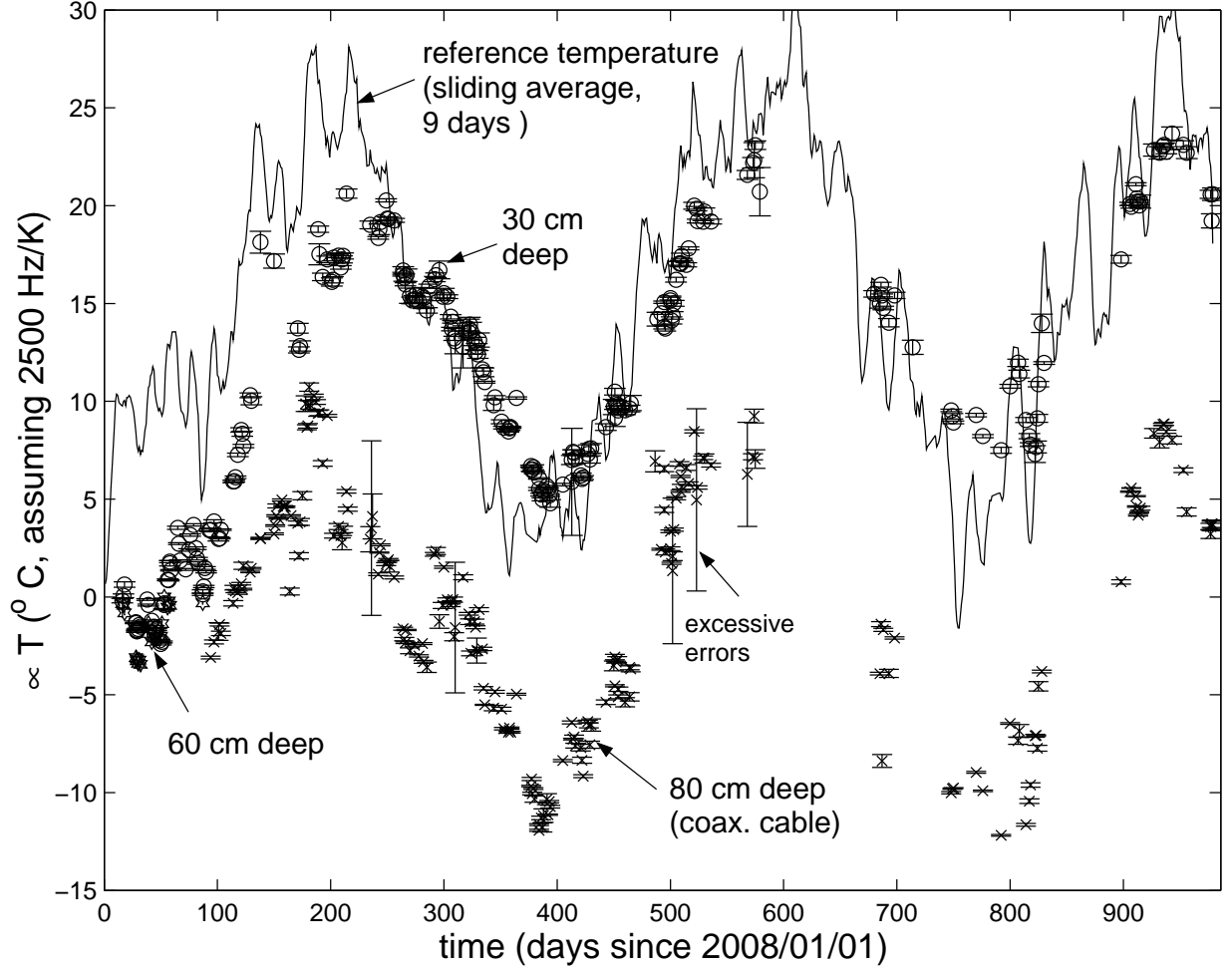


FIG. 2: Evolution over more than two years of the temperature of buried sensors at depths between 30 and 80 cm. The sensors survived this environment for the duration of this experiment, with no noticeable drift or loss in RF link quality, while providing data consistent with surface temperatures. Only *relative* temperatures are provided by the sensors since no calibration was performed prior to the experiment: the buried sensor temperatures have been shifted with respect to the averaged air temperature for clarity, while qualitatively exhibiting similar trends after processing the mean air temperature through a 9-day running average (thick solid line, maximum and minimum daily temperature obtained from the web site referenced in the main text. Data quality is assessed through the standard deviation of the 20-s dataset gathered during each measurement: a few unsuitable data with excessive deviation are displayed for demonstration purpose (days 230 or 500 for example).

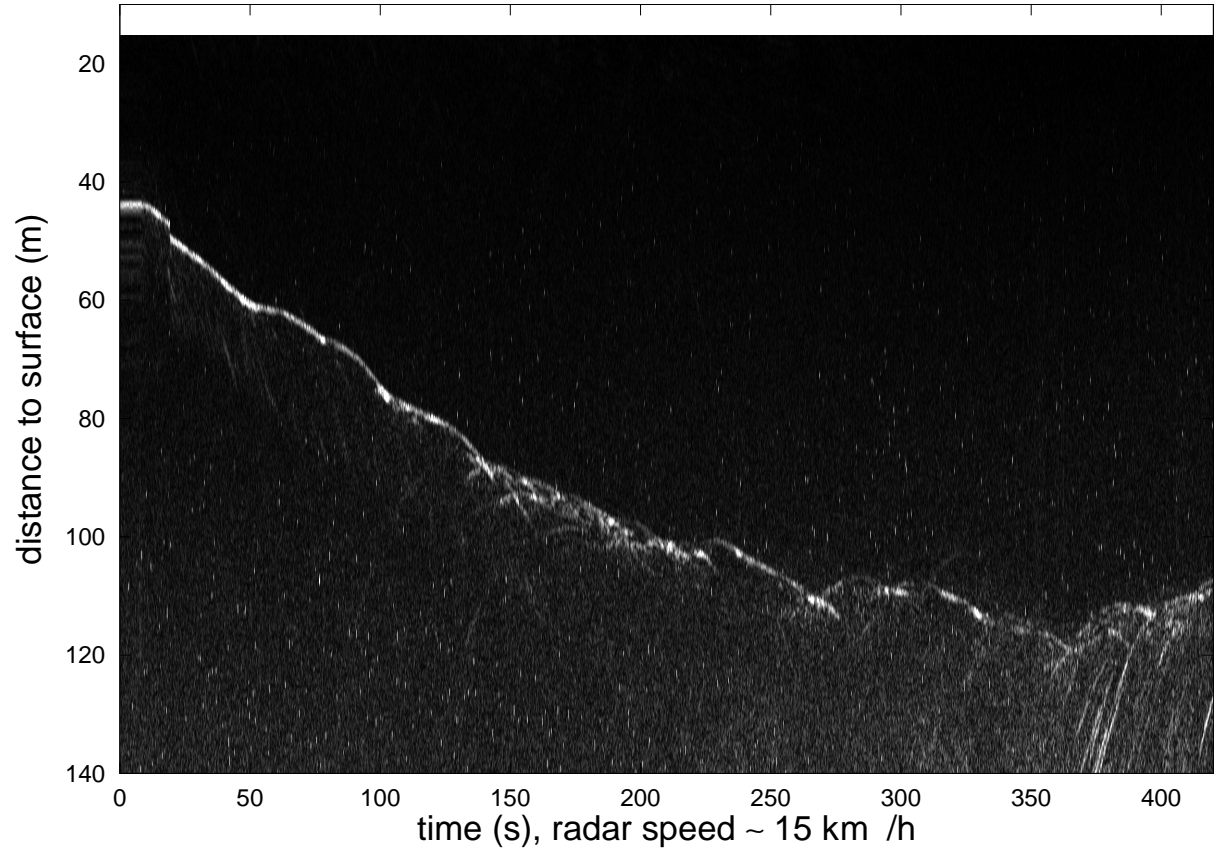


FIG. 3: 100 MHz ground penetrating RADAR scans of the ice-rock interface: the signal is detected for an interface deeper than 100 m. The raw RADAR signal were processed using Aslak Grinsted's `processradar.m` Matlab tool. Data acquired on the Austre Lovénbreen glacier (Spitsbergen, Norway).

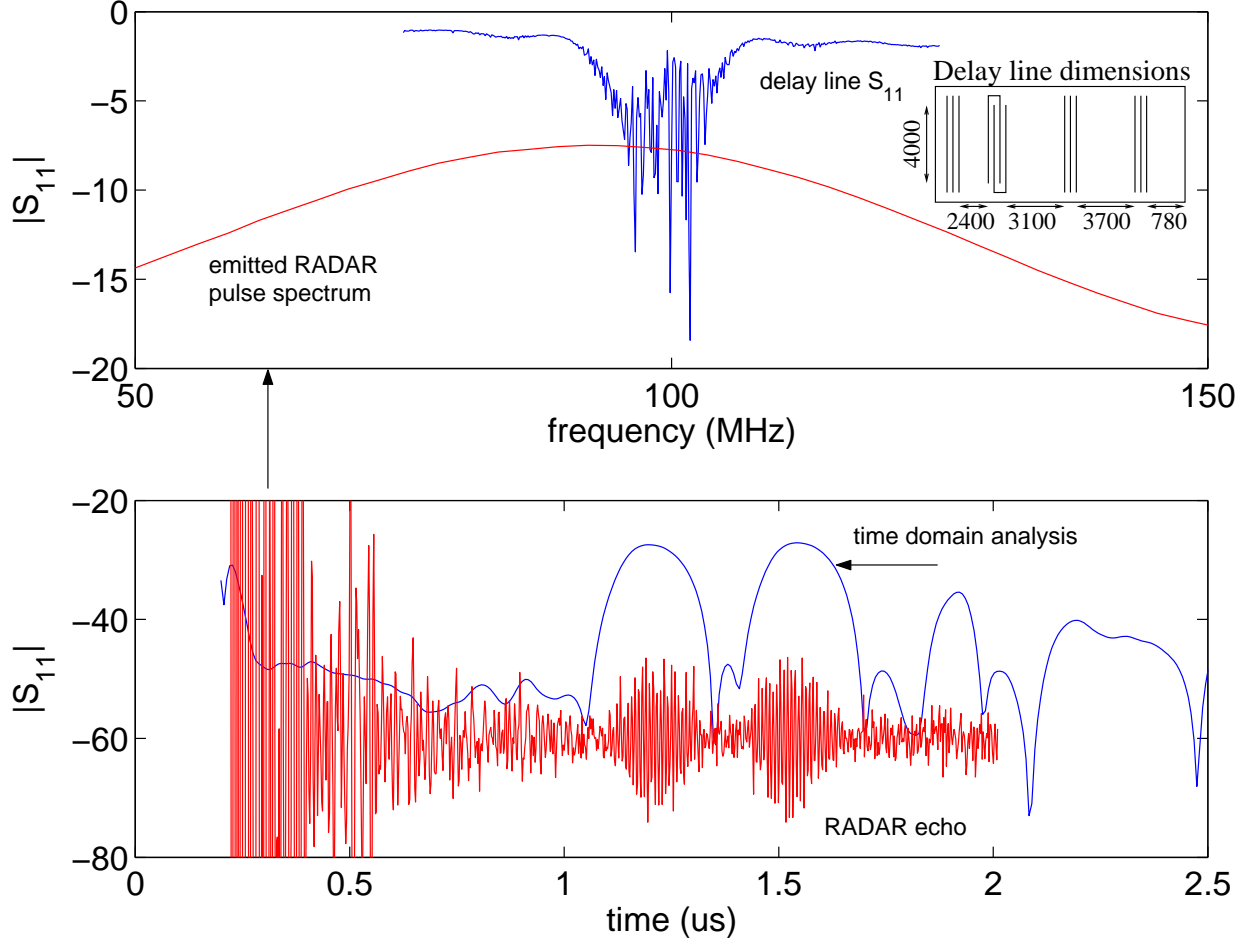


FIG. 4: Frequency domain (top) and time domain (bottom) characterization of a 100 MHz, dual mirror delay line. The blue lines are characterization on a Rohde & Schwartz network analyzer under a probe station, with the time domain signal obtained as the inverse Fourier transform of the frequency domain characterization. The red signal in the time domain plot (bottom) is the RADAR echo observed when locating a sensor 50 cm away from the receiving antenna. The red signal in the frequency domain plot is the power spectrum of the RADAR pulse, obtained by Fourier transform of the emitted pulse: although the central frequency is dependent of the dielectric environment of the emitting antenna, a large fraction of the emitted pulse overlaps the frequency region of the delay line. Top-right inset: dimensions of the delay line, transducers and mirror position (all dimensions in micrometers). One mirror is located to the left of the transducer, two mirrors are located on the right. Each side of the IDT transducer is connected to one branch of a dipole antenna through silver-epoxy bonding.

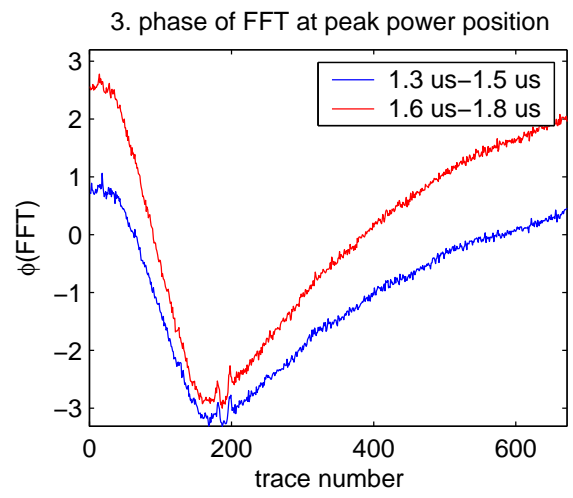
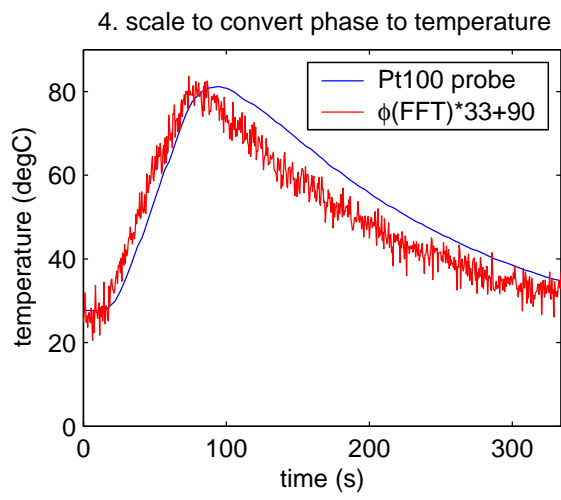
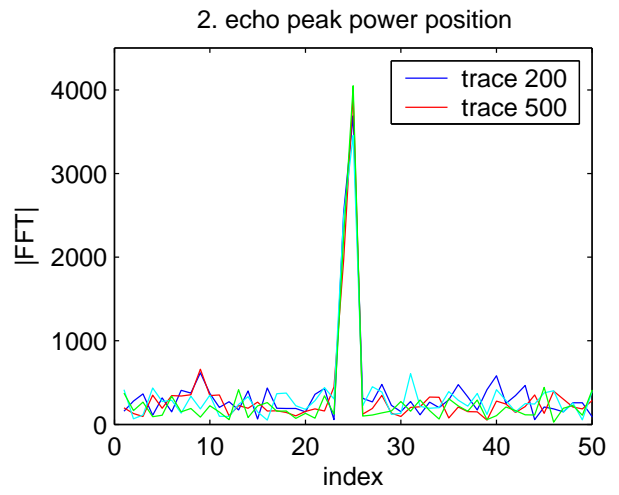
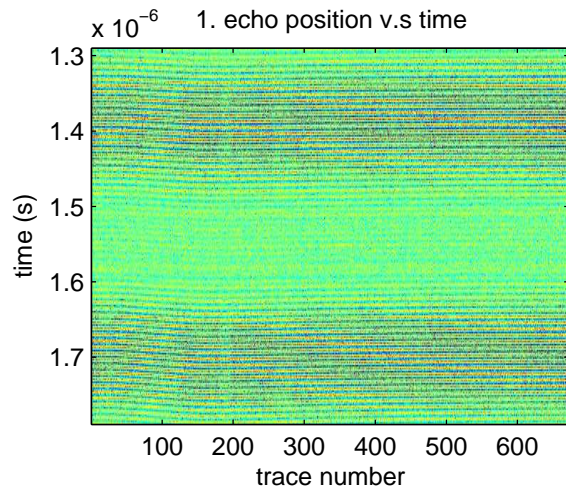


FIG. 5: Top left: the raw color-coded time evolution of the recorded RADAR echo magnitude between $1.0 \mu\text{s}$ and $1.3 \mu\text{s}$ after the excitation pulse was emitted. The sampling is performed at 500 MHz, or 5 times the frequency of the signal of interest. Top-right: identification of the frequency component (index) representative of the delay line, here visible as a maximum of the magnitude of the Fourier transform of the points from 0.9 to $1.1 \mu\text{s}$ (first echo) and 1.2 to $1.4 \mu\text{s}$ (second echo). We observe that this frequency component of interest does not change with temperature (*i.e.* is independent on the trace number). Bottom right: time-evolution of the unwrapped phase of the Fourier transform at frequency abscissa 25 as identified from the top-right graph. Bottom-left: time evolution of the phase difference between the first and second echoes, after scaling and translation to match the reference temperature curve recorded with a Pt100 probe located next to the delay line. During this whole experiment, the receiving antenna is located 1 m from the emitting antenna, and the sensor is 50 cm from the receiving antenna *away* from the emitting antenna.

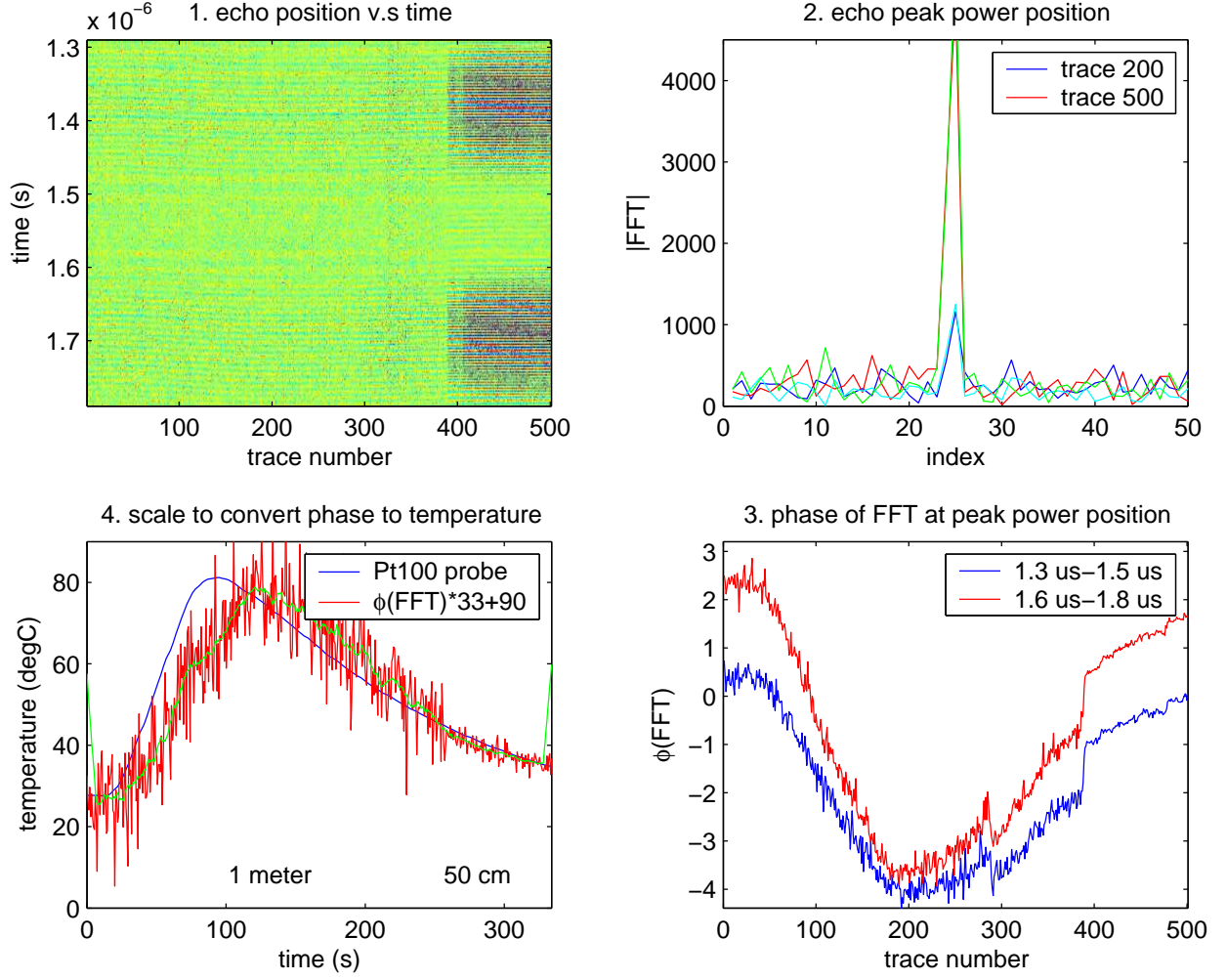


FIG. 6: The graph sequence and analysis is the same than the one described in the caption of Fig. 5. Here, however, the sensor is first located 1 m from the receiving antenna, away from the emitting antenna, and brought closer to 50 cm of the receiving antenna at trace number 400. This distance change is observed as an increase of the magnitude of the signal of interest (top right graph, magnitude of the Fourier transform of the echo), a phase shift in the bottom graph affecting both echoes in the same way, and a decrease of the temperature estimate standard deviation (bottom-left graph).

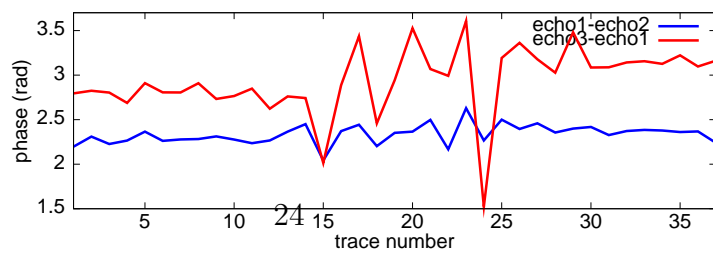
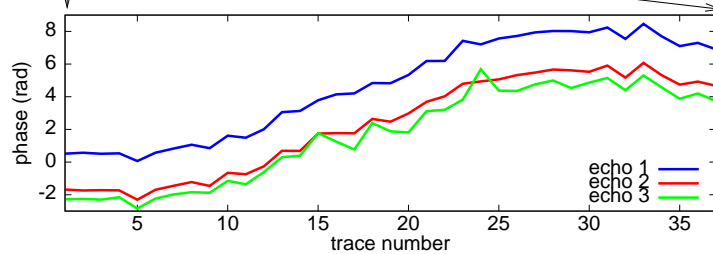
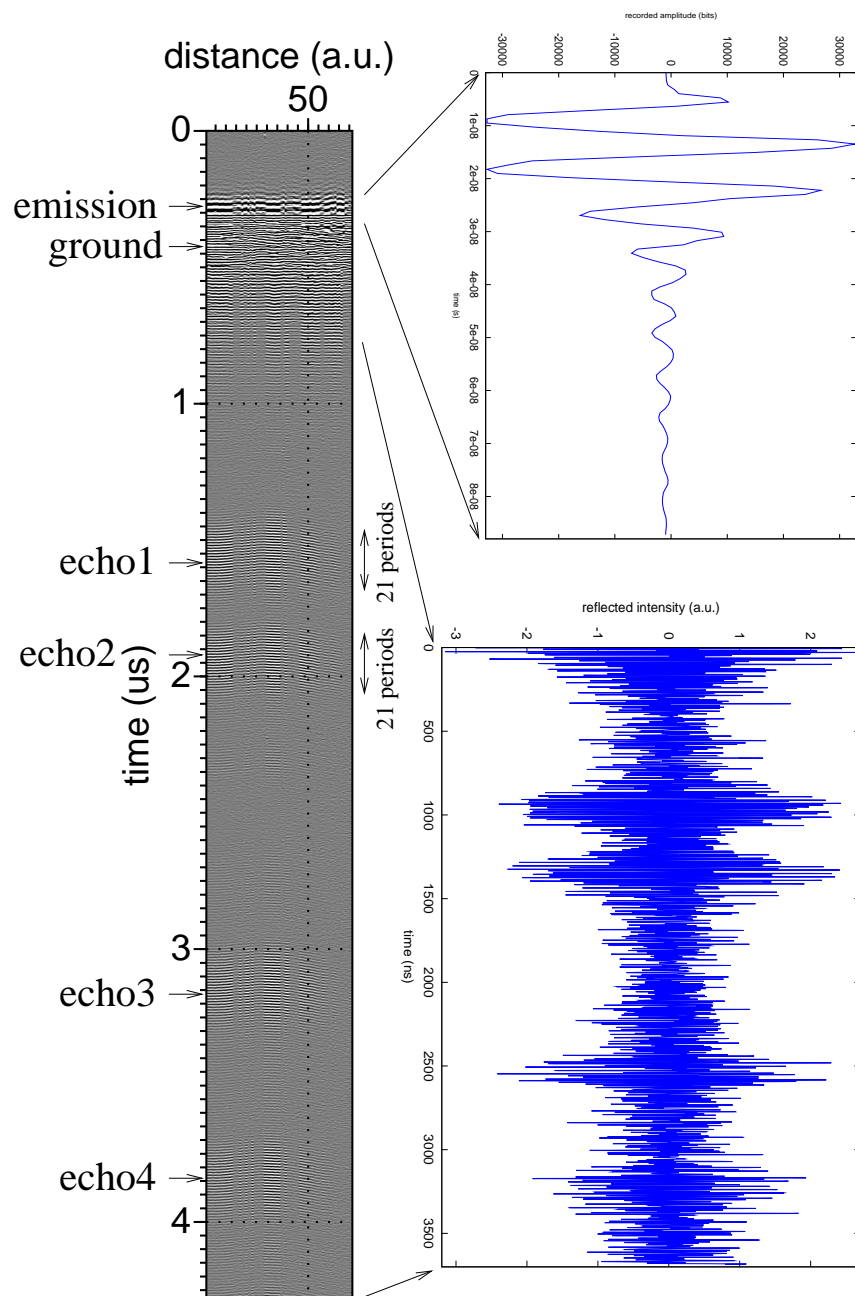


FIG. 7: Signal acquired while scanning a 100 MHz GPR unit over a sensor buried 2.20 m deep in snow. The emitted pulse exhibits ringing due to impedance mismatch, a condition degrading depth resolution but favorable to efficiently load the acoustic delay line. The recorded signal clearly displays four echoes, the first three being used to extract the physical quantity under investigation. The absolute phase with respect to the emitted pulse is dependent on antenna position and constantly rises as the RADAR is brought close to the sensor, but the phase *difference* is independent on antenna position and is representative of the physical quantity under investigation. As expected, each echo is made of 21 oscillations, which is equal to the number of electrode pairs in the transducer. The “inverted” hyperbola shape of the echoes is an aliasing artifact when displaying the data.

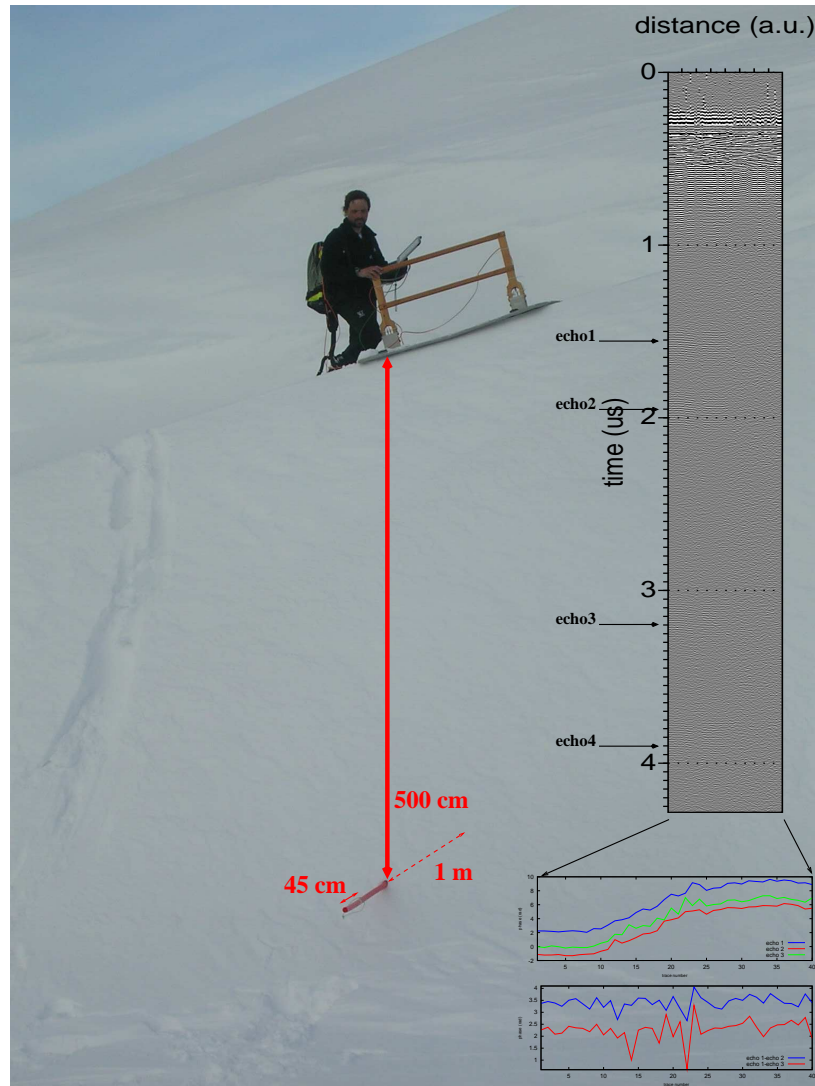


FIG. 8: Experimental setup for recording signals from a sensor while scanning a 100 MHz GPR unit over a sensor buried 5 m deep in snow. The emitted pulse exhibits ringing due to impedance mismatch, a condition degrading depth resolution but favorable to efficiently load the acoustic delay line. The recorded signal clearly displays four echoes, the first three being used to extract the physical quantity under investigation.

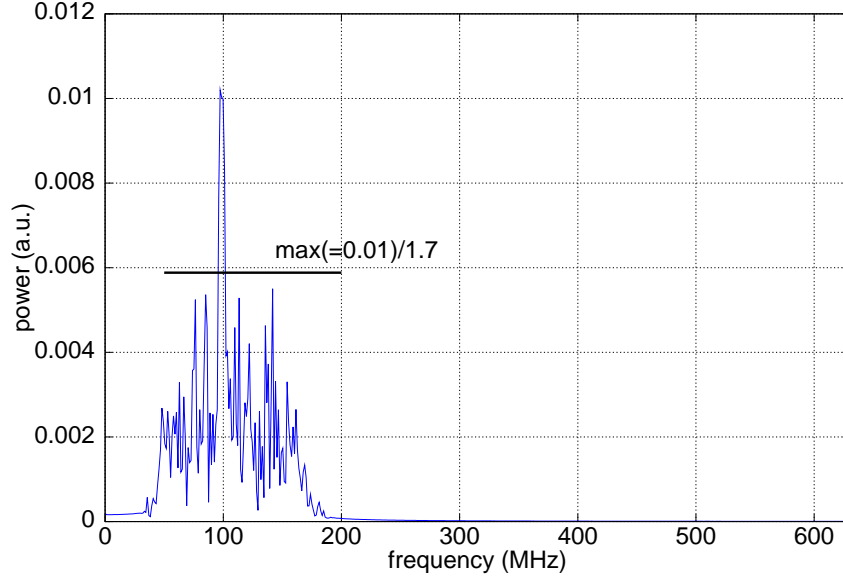


FIG. 9: Fourier transform of the returned echoes for a sensor buried 5 m deep in snow: the spectrum is given in linear arbitrary unit, exhibiting a signal to noise ration above 1.7. This measurement indicates that the echo detection should be possible at a distance between the GPR unit and the sensor of 40 m. Indeed, following the RADAR equation, and assuming only propagation loss, the returned power decreases as the fourth power of the distance, and $8^{1/4} \simeq 1.7$.